The role of Cerium, Europium and Erbium doped TiO2 photocatalysts in water treatment: A mini-review

Chemical Engineering Journal Advances 10 (2022) 100268

Contents lists available at ScienceDirect

Chemical Engineering Journal Advances

journal homepage: www.sciencedirect.com/journal/chemical-engineering-journal-advances

The role of Cerium, Europium and Erbium doped TiO_2 photocatalysts in water treatment: A mini-review

Erik Cerrato [b], Elisa Gaggero [a], Paola Calza [a], Maria Cristina Paganini [a,*]

[a] Department of Chemistry and NIS, University of Turin, Via P. Giuria 7, 10125 Torino, Italy
[b] INRIM Istituto Nazionale di Ricerca Metrologica, I- 10135 Torino, Italy

A B S T R A C T

Heterogeneous photocatalysis is a promising environmentally friendly strategy for removing contaminants of emerging concern from water, with titanium dioxide being the most studied and exploited photocatalyst, thanks to its good optical and electrical properties. However, one of the main drawbacks linked to its use is the limited absorption of sunlight; several strategies have been explored to enhance the absorption in visible light region and, among them, the doping with elements belonging to the lanthanoid series is particularly attractive. This review focuses on these systems analysing the cases of Cerium, Europium and Erbium doped TiO_2 and giving an overview on the structural, optical and electronic characteristics of these materials. Synthesis procedures, inserted dopant percentages, structural and optical properties and the main operating conditions adopted in the photodegradation studies are considered. Particular attention is devoted to unravel the effect induced by the introduction of lanthanoids on the energy gap, on the recombination rate of photogenerated electron-hole pairs and on the inhibition of phase transition from anatase to rutile.

Introduction

In recent decades we are witnessing rapid changes in the world we live in: rapid human population growth, urbanization, the increase of areas dedicated to agriculture and climate change result in the scarcity of clean water resources, making the resolution of the water crisis a problem of paramount importance.

In addition, a widespread contamination of water due to the conveyance through various routes of potentially toxic elements (PTEs) and contaminants of emerging concern (CECs) is attested.

CECs encompass a wide range of organic molecules, all sharing poor and not definitive removal during conventional wastewater treatment plants, which include percolating filters or activated sludge, chemical-physical treatments such as clarifloculation and mechanical treatments such as filtration on activated carbon or sand filters. This results in their release into the environment [1], where they can cause serious damage to aquatic ecosystems as well as being harmful to human health, since their carcinogenicity, teratogenicity, mutagenicity and their interference with the endocrine system have been assessed by several studies [2, 3].

Advanced oxidation processes (AOP) represent an efficient and inexpensive method for the degradation of organic pollutants [4–6]. Among these techniques, the photocatalytic process by using transition metal oxide semiconductor photocatalysts has been widely developed and found application in the abatement of CECs from aqueous matrices [7, 8]. In particular, titanium dioxide nanoparticles exhibit the highest efficiency in wastewater contaminants removal and is particularly attractive as being nontoxic, inexpensive, eco-friendly, and stable over a wide pH range. TiO_2 nanoparticles exist in three crystallographic phases, namely rutile (thermodynamic phase), anatase, and brookite (metastable phases). Among these, anatase is the most stable and efficient in photocatalytic applications due to its less compact structure [9] and to a higher hydroxylation of the surface-facilitated adsorption of oxygen in the form of O_2^- or O^- [10]. The mechanism underlying semiconductors photocatalysis involves the absorption of light energy, which, if greater than the energy gap of the material, leads to the photogeneration of electron/hole pairs. Electrons and holes thus generated then migrate to the surface, where they can react with the adsorbed species, such as electron acceptors or donors. Therefore, the holes in the VB can react with water with the formation of highly reactive hydroxyl radicals (• OH) that have very high oxidizing potential; at the same time dissolved oxygen acts as an acceptor of electrons for the formation of the oxygen ion superoxide ($^{\bullet}O_2^-$), which is also highly reactive and capable of oxidizing organic molecules [11]. The energy gap of TiO_2 in anatase phase is equal to 3.2 eV, therefore it is photoactive in the UV region ($\lambda <$ 388 nm) and its application is limited by a very poor response to visible light. In order to use solar energy efficiently and to reduce the electron-hole recombination, various strategies have been developed

* Corresponding author.
E-mail address: mariacristina.paganini@unito.it (M.C. Paganini).

https://doi.org/10.1016/j.ceja.2022.100268

Available online 16 February 2022

such as dye sensitization [12, 13], noble metal loading [14, 15], transition metal addition [16–18], heterojunctions [19–21] and non-metal doping [22–24]. Lanthanoid ion doping is a versatile strategy to modulate the optical response and improve the photocatalytic properties of TiO_2. Lanthanoids comprehend fifteen elements, namely La, Ce, Pr, Nd, Pm, Sm, Eu, Gd, Tb, Dy, Ho, Er, Tm, Yb and Lu in the periodic table. They own unique chemical properties for photocatalytic applications and exhibit luminescent properties resulting from electronic *f-f* transitions in their partially filled *f* orbitals, protected by the electronic shield provided by the extern and fully filled $5s^2$ and $5p^6$ shells. TiO_2 doping with lanthanoids allows the redshift of the absorption, the increase of the transition temperature from anatase to rutile and result in the narrowing of the band gap.

The aim of this mini-review is to investigate how doping with lanthanoids modifies the properties of titanium dioxide and the mechanism of light absorption and charge carriers separation with the consequent variation of the photocatalytic efficiency toward the degradation of pollutants in wastewater. In particular, three elements belonging to the class of lanthanoids are examined: cerium, europium and erbium. The selection of the elements is due to the intention to cover the entire series of lanthanoids, taking into consideration an element at the beginning, one in the middle and one at the end of the series, with the aim of describing the peculiarities resulting from the different filling of orbitals 4f.

Most of the photodegradation studies available in literature were conducted on dyes, both because they represent a class of organic pollutants that are very harmful to the environment, and because their degradation can be easily followed via spectrophotometric measurements; however, several studies on other emerging contaminants have been selected, as reported in the following tables, where the main details and operating conditions in which the studies were carried out are also summarized.

Ce-doped tio₂

Despite TiO_2 represents the most studied and used photocatalyst, the Ce-doped TiO_2 system has not relished the same application if compared to other doped-TiO_2 materials or to the bare oxide in the photodegradation of contaminants in aqueous environment. This probably derives from the fact that the identification of the actual cerium character in the titanium dioxide has been incredibly harsh and a satisfying and conclusive model of the working mechanism upon light absorption is still absent. Nevertheless, varied investigations exploring the mineralization upon visible and UV irradiation of various harmful pollutants in wastewater such as industrial dyes [25–38], aromatic compounds [39–41] and herbicides [42–44] by Ce-TiO_2 have appeared since the early 2000s, as listed in *Table 1*.

The uncertainties regarding the role of Ce range from the structural to the electronic features. However, what emerges is that the presence of cerium stabilizes the anatase phase at higher temperatures, so inhibiting the phase transition to rutile, regardless the synthetic approach employed (*Table 1*). In this framework, the spectroscopic works of *Lopez* et al [45]. and *Fang* et al [46]. were pivotal in determining the site in which cerium ions localize during the synthesis process, namely in the TiO_2 shallow oxygen vacancies: this occurrence would establish the formation of new Ti-O-Ce bond, that would transfer the anatase-to-rutile phase transformation at higher temperature (up to 1000 K).

One of the most controversial aspect remains the incorporation of $Ce^{3+/4+}$ ions in TiO_2 lattice rather than the formation of a CeO_2-TiO_2 biphasic solid. Most of the authors agree with the fact that due to the different symmetry in which the two oxides crystalize (tetragonal for TiO_2 and cubic for CeO_2) and due to the different cationic size (Ce^{4+} 0.92–0.97 Å; Ce^{3+} 1.14 Å, Ti^{4+} 0.61 - 0.68 Å) the insertion of Ce ions in the TiO_2 lattice seems somewhat unlikely. However, also in large Ce contempt, any signals attributable to some cerium phases (in oxide form or solid solution) has been frequently detected: just in few cases the biphasic interface CeO_2-TiO_2 or the $Ce_xTi_{1-x}O_2$ solid solution have been hypothesized [31, 34, 37, 41]. Several times the absence of XRD reflections referred to cerium phases has been justified asserting that cerium atom might be located in grain boundaries of TiO_2 nanocrystals [30, 41] or that the CeO_2 and/or Ce_2O_3 phases, precipitated during the synthesis, is too much dispersed and amorphous to be detected via XRD analysis [28, 32, 36, 47, 48]. Due to the supposed stabilization of cerium atoms at the grain boundaries, the average crystal size of the produced nanoparticles decreased with increasing cerium percentage, with a consequent enlargement on the exposed specific surface area. Still referred to this aspect, *Makdee* et al [26]. provided Williamson-Hall analysis evidencing an increased lattice strain with the increment of cerium content in the solid. Similar outcomes have been obtained by means of Raman spectroscopy, in which the shift of the peaks at 392 and 511 cm^{-1} (typical of anatase phase) to higher values has been interpreted as a perturbation caused by the presence of Ce ions or cerium in its oxide forms, as shown in Fig. 1A [43, 44]. This variation in the Raman acquisitions respect to unperturbed TiO_2 anatase might also suggest a substitution at the interface of the Ti^{4+} cations with Ce^{4+} cation, establishing new Ti-O-Ce bonds, as also supported by theoretical calculations [45].

A common aspect coming out from the literature concerns the narrowing of the TiO_2 band gap with the increase of Ce content, shifting the absorption edge from UV to visible photon absorption, up to 450 nm, as noticeable in Fig. 1B). The resulting red-shift has tentatively been explained by claiming the possible charge transfer between the *4f* levels of Ce, acting as localized intraband gap states or as shallow CB donor levels, and the electronic levels of the band structure [25, 26, 30, 33]. Some authors sustained that the improved visible photon absorption would originate from the electronic transition of the CeO_2 and/or Ce_2O_3 at the interface with TiO_2 or still between impurity levels induced in the band gap by the instauration of new chemical bonds at the interface of the Ti-O-Ce [28, 32, 47].

Analysing the mechanism involved in the Ce-doped TiO_2 system upon irradiation, several authors claim an electron scavenger action undertaken by the Ce^{3+}/Ce^{4+} redox couple.

Accordingly, the *4f levels* of cerium, both as isolated ions at the TiO_2 surface or in its oxide forms would guarantee an inhibition of the electron-hole pairs recombination. Moreover, acting as a stronger Lewis acid than O_2, the photoexcited electrons from TiO_2 VB can be easily captured by Ce ions and subsequently be transferred to molecular oxygen in order to form the radical species $^{\bullet}O_2^-$ [27, 29, 30, 33, 36, 48]. In this framework, a too high dopant contempt would result in a high number of recombination centres, thus suppressing the photodegradation ability. Different studies assert that the stabilization of Ce at the surface or at the interface of TiO_2 might increase the amount of lattice defects, particularly of the oxygen vacancies: these last, placed at the bottom of the CB, could still act as electron scavengers further enhancing the electron-hole separation and then the photocatalytic capability of the modified material, as reported in the model in Fig. 2 [26, 32, 43].

As a conclusive remark about the improved photocatalytic performance of Ce-doped TiO_2, it is worth mentioning the study performed by the group of *Giamello* et al [50].; in their investigations they were able to identify a further phase coming out from the mixture at a 50% ratio Ce: Ti. In details, by means of μ-Raman spectroscopy the onset of a new set of lines were assigned to the cerium titanate $Ce_2Ti_2O_7$ phase, not previously detected by XRD and indicating an intimate interaction between ceria and titania into the mixed material [50]. Cerium titanate shows a pyrochlore structure, containing Ce^{3+} and Ti^{4+} ions in eightfold and six fold coordination, respectively [51]. This compound exhibits a brown coloration due to the presence of Ce^{3+} ions having one electron in the strongly localized *4f* orbitals: the *4f* electron of Ce^{3+} generates a pair of spin-orbit split states ($^2F_{5/2}$ $^2F_{7/2}$). Thus, the same type of spin-orbit split state can be assumed to be present, which can absorb visible light via a charge transfer transition from *4f* to the empty orbitals of Ti^{4+}.

Table 1
Ce concentration, structure, morphology and reaction condition used for the degradation of various pollutants for different Ce-doped TiO_2 studies.

Synthetic route	Ce contempt, %	Structure and morphology	Irradiation source (Power, W)	Tested pollutant	Pollutant, concentration, mg/L	Photocatalyst, concentration, mg/L	Solution volume, mL	Best Degradation efficiency	Ref.
Sol-gel	0.5–40	Anatase. Biphasic CeO_2-TiO_2 for 40% Ce. Nanospheres	UV light (λ_{max} = 254 nm, 250 W)	Deoxynivalenol (DON)	5	125	20 mL	0.5% Ce, 85% after 240 min	[41]
Sol-gel	2.5–10	Anatase	UV light (200 W)	2,4-Dichlorophenoxyacetic (2,4-D-acid)	30	200	250 mL	5% Ce, 100% after 240 min	[44]
Precipitation	0.1–1	Anatase Nanotubes	UV–Vis (125 W)	Glyphosate (Gp)	17	200	500 mL	0.15% Ce, 80% after 1h	[42]
Sol-gel	0.2–2	Anatase	Vis-light (100 W)	2-Mercaptobenzothiazole (MBT)	21.7	1000	250 mL	0.7% Ce, 95% after 100 min	[39]
Hydrothermal	0.15–1	Anatase	Vis-light (λ_{max} = 620 nm, 41 W)	Methylene Blue (MB)	20	500	750 mL	0.5% Ce, 95% after 160 min	[49]
Sol-gel + Hydrothermal	0.06–0.4	Anatase. Nanotubes	Vis-light ($\lambda \geq 400$ nm, 300 W)	MB	200	150	100 mL	0.12% Ce, 85% after 2h	[29]
Hydrothermal	0.1–1	Anatase Nanotubes	Vis-light ($\lambda \geq 420$ nm, 300 W)	MB	10	1000	100 mL	0.1% Ce, 65% after 4h	[48]
Hydrothermal	0.05–1	Anatase	UV–vis light (λ_{max} = 420 nm, 250 W)	MB, Imidacloprid (IMCD) and Quinalphos (QP)	20	500	10 mL	0.2% Ce, 100% for MB, 90% for QP and 88% for IMCD after 8h	[43]
Sol-gel	0.1–8	Anatase	UV light (125 W)	Methyl Orange (MO)	10	300	100 mL	0.5% Ce, 86.9% after 210 min	[26]
Sol-gel	0.5–2.5	- Porous structures	UV light	MO	–	20	250 mL	1.5% Ce, 87% after 6h	[27]
Sol-gel	0.15–0.45	Anatase	Vis-light (8 W)	MO	10	1000	50 mL	0.35% Ce, 70% after 1h	[32]
Sol-gel	7–50	Biphasic CeO_2-TiO_2 for 15, 25 and 50% Ce	Direct sun light	MO	20	5000	50 mL	11% Ce, 86.8% after 4h	[34]
Sol-gel	0.1–0.3	Anatase	Vis-light ($\lambda \geq 410$ nm, 150 W)	MO	500	2000	100 mL	0.2% Ce, 30% after 4h	[36]
Sol-gel	0.6	Anatase and Rutile	UV-light	Phenol (Ph)	50	400	500 mL	94% after 3h	[40]
Sol-gel	1–3	Anatase, Brookite and $Ce_xTi_{1-x}O_2$	UV–Vis (250 W)	Reactive brilliant X-3B (X-3B)	50	350	200 mL	2% Ce, 45% after 80 min	[37]
Esterification	0.2–1	Anatase Spheres	Vis-light (300 W)	Rhodamine B (RhB)	20,000	1000	50 mL	0.4% Ce, 80% after 7h	[28]
Sol-gel	0.5–3	Anatase	UV–Vis (500 W)	RhB	10	500	100 mL	1.5% Ce, 70% after 6h	[30]
Hydrothermal	–	Biphasic CeO_2-TiO_2. Nanocubes	Vis-light ($\lambda \geq 400$ nm)	RhB	479	25,000	30 mL	93% after 2h	[31]
Hydrothermal	1–4	Anatase Squama like nanocomposite	UV–Vis (40 W)	RhB	4.8	200	100 mL	3% Ce, 86.7% after 2h	[33]

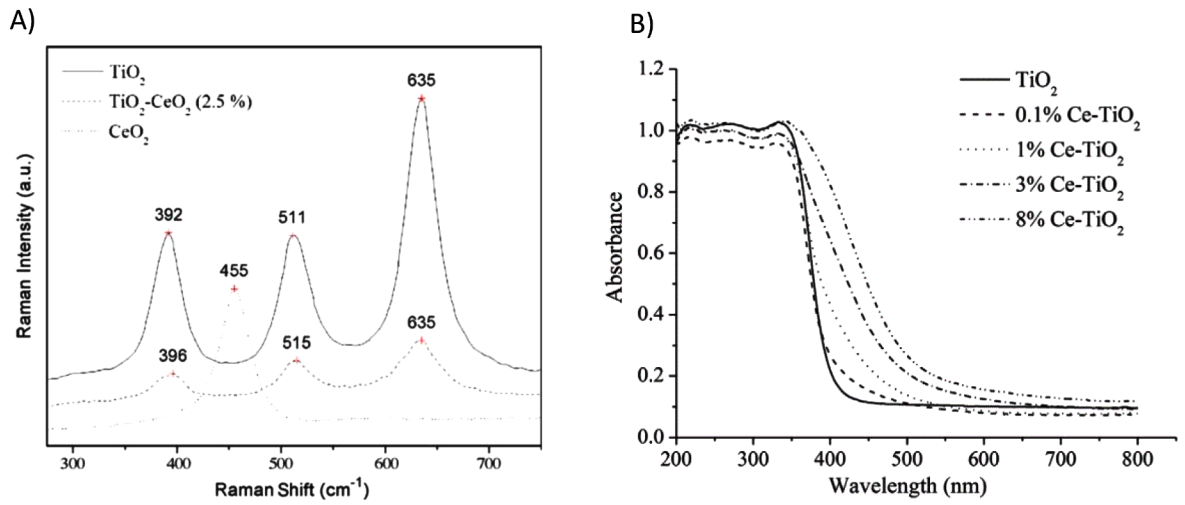

Fig. 1. A): Raman spectra for the TiO_2, TiO_2–CeO_2 and CeO_2 samples in the 300–750 cm^{-1} region [44]. B): UV–Vis DRS spectra of TiO_2 and all Ce-doped TiO_2 samples [26].

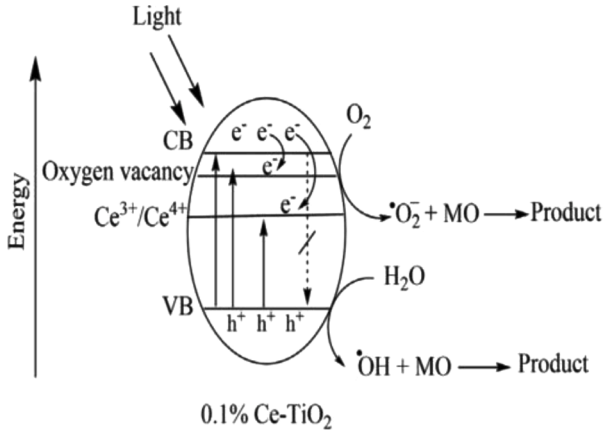

Fig. 2. The mechanism of methyl orange dye degradation over 0.1% Ce-doped TiO_2 under UV light irradiation [26].

Accordingly, the brownish yellow coloration assumed by the Ce-TiO_2 samples as well as the narrowing of the material band gap would be explained by the presence of $Ce_2Ti_2O_7$ solid solution. However, further investigations are extremely needed in order to verify if the real photocatalytic engine of the Ce-TiO_2 activity can be appropriately assigned to the presence of the pyrochlore structure.

Eu-doped tio₂

Some preliminary structural information, useful for identifying which factors determine the greater photocatalytic efficiency of Eu-doped TiO_2, can be obtained from XRD patterns.

Doping with Eu(III) ions has been found to inhibit the anatase-to-rutile phase transformation and to force the formation of a mesoporous structure with significantly increased surface area and pore volume [52, 53]. This effect was explained by *Leostean* et al [53]. in terms of competition between the simultaneous TiO_2 crystallites formation and the Eu insertion: higher Eu amount in the precursor mixture reduces the rate of crystallite formation and favours the doping process. In most of the studies the diffractograms of Eu-doped titania samples have exclusively revealed the existence of TiO_2 anatase phase [52, 54–61], which is superior to other phases of TiO_2 in terms of photocatalytic response.

As regards the substitution of Eu^{3+} in the crystal lattice of TiO_2 or the formation of a secondary phase of Eu_2O_3, conflicting results exist in the literature. *Khade* et al [56]. and *Al-Shomar* et al [60]. did not observe any characteristic peaks of europium oxide in XRD pattern of Eu–doped TiO_2, probably due to the very small content of Eu, which can be incorporated into TiO_2 lattice to substitute Ti^{4+}. They also reported that the diffraction peaks of Eu-doped TiO_2 became wider and of lower intensity compared to pristine TiO_2, which indicates that doping of Eu^{3+} reduces the crystallite size; in addition, the segregation of Eu^{3+} at the grain boundary of TiO_2 prevents their growth. The average crystallite size decreased linearly with increasing Eu^{3+} concentration due to the production of nucleation centers on the surface when a greater amount of dopant was present. In terms of photocatalytic efficiency, the smaller crystallite size is an advantage since the photogenerated charge carriers have a higher probability to reach the surface before undergoing the recombination process.

The diffraction peak positions remained unaltered for un-doped and Eu-doped TiO_2 nanopowder samples prepared by *Paul* et al [62].. The intensity of the diffraction peaks gets suppressed with the increase in dopant concentration, so bringing to a loss of crystallinity due to lattice distortion, suggesting that Eu^{3+} underwent substitutional doping into the titania host lattice. On the other hand, it must be considered that the ionic radius of Eu^{3+} (0.095 nm) is larger than that of Ti^{4+} (0.068 nm), therefore it is difficult for Eu^{3+} to enter the TiO_2 lattice, and especially when increasing the percentage of doping, it is more likely that it is bound in interstitial positions or on the surface of the TiO_2 nano crystallites [52, 63–65].

Serga et al [65]. used the extraction-pyrolytic method (EPM) and mixtures of Ti- and Eu-containing organic extracts based on valeric acid as precursors for fabrication of nanocrystalline TiO_2-based powders with different Eu content (0.5, 5, 50 mol%): they evidenced the formation of nanocrystalline TiO_2 powder, consisting of anatase and rutile polymorphs and an additional phase of europium oxide Eu_2O_3. Interestingly, for Eu content equal to 5 mol% the beginning temperature for anatase-to-rutile phase transformation shifts from 550 °C for pure TiO_2 to 750 °C. The reasons for a more hindered transformation from anatase to rutile lie in the obstruction of ionic mobility due to interstitial europium which prevents the cleavage and rearrangement of Ti-O bonds and in the inhibition of the growth of anatase particles caused by the presence of Eu_2O_3 on the surface. This hampers agglomeration and prevents the attainment of the critical size of the anatase particles (14 nm) for the formation of rutile. If Eu_2O_3 is precipitated on the titania surface by means of liquid phase plasma (LPP) [63], Ti^{4+} can be converted to Ti^{3+} by charge compensation and acts as a trap increasing the rate of adsorption and reducing the recombination of photogenerated

electron-holes. The photocatalytic activity is proportional to the amount of Eu precipitated on the TiO_2 surface; when Eu is precipitated on the surface, a new energy level is formed below the CB of TiO_2, and the band gap energy decreases allowing excitation by blue light absorption.

Generally, the main problems encountered in using TiO_2 as a photocatalyst are the lack of response to visible light and the high recombination rate of photogenerated charge carriers that hinder the photocatalytic performance. However, Eu doping leads to the creation of impurities and additional energy levels thus lowering the energy gap. The absorption spectra of Eu-doped TiO_2 samples highlight a broad absorption edge in the visible region that enhance with higher Eu concentration, whereas the energy band gap decreases as the Eu loading increases [64]. Moreover, the UV–vis analyses in several studies [56, 63, 65] show that Eu^{3+} ion doping leads to red shift of absorption profile indicating the charge transfer transition between the lanthanoid and TiO_2 conduction band or valence band.

Looking at the photocatalytic degradation of different molecules (mainly dyes) reported in literature and summarized in Table 2, it is quite clear that Eu-doped TiO_2 is more efficient than the un-doped oxide. Besides the improved absorption and charge separation, due to *4f* electron configurations of Eu, and the enhanced photocatalytic activity of TiO_2 under vis irradiation due to red shifts of the optical absorption edge, some factors come into play in determining the photocatalytic efficiency. For instance, an optimal doping percentage exists, since the proper amount of Eu^{3+} ion concentration in TiO_2 can effectively trap the photo generated electrons which can immediately transferred to oxygen adsorbed on the surface of TiO_2 leading to a bigger quantity of $^{\bullet}OH$. If Eu^{3+} ions concentration exceed the optimum value, they can cover the surface of TiO_2 bringing to a decrease in the concentration of photogenerated charge carrier species and therefore in photocatalytic activity [56].

In literature numerous examples of synergistic or co-catalytic effect of co-doped or hybrid systems based on europium and TiO_2 are reported. The photocatalytic activity of (Eu, Sm)-codoped TiO_2 loaded on GO nanocomposite was investigated by *Gohr et al* [54]. who found that the high specific surface of the GO and its functional groups containing oxygen allows to obtain a higher absorption; moreover, GO acted as photosensitizer and electron scavenger, while doping with an appropriate amount of Sm^{3+} and Eu^{3+} led to a further improvement of the photocatalytic activity by expanding the amount of electron-hole pairs. (Eu, N)-codoped TiO_2 prepared by *Jiang* et al [66]. using plane-wave pseudopotential method and (Eu, N)-codoped TiO_2/sepiolite nanocomposites fabricated by *Zhou* et al [67]. showed an enhanced photocatalytic activity due to the synergistic effect of the Eu and N that led to high crystallinity of anatase phase, lattice distortion, band gap narrowing, and easier separation electron-hole pairs. In addition, the visible-light photocatalytic activity was improved in accordance with the significant red-shift of absorption edge in the optical absorption spectra. The cooperative action of the co-dopants was observed in (Au, Eu)codoped-TiO_2 by *Lin* et al [68]. who hypothesized that the visible light photogenerated electrons may be transfer from the conduction band of TiO_2 to adjacent Au nanoparticles deposited on the surface of Eu-doped TiO_2, with consequent decrease of the recombination rate of electron-hole pairs as schematized in Fig. 3. They confirmed their thesis by studying the (Au, Eu)-doped TiO_2 by XPS after its use in the photocatalytic degradation of Rhodamine B dye. The sample, after photocatalysis under visible light irradiation, exhibited a lower binding energy of Au 4f (from 83.5 eV to 83.25 eV), suggesting the relatively higher surface electron density of Au. This result proved that Au NPs deposited on the surface of Eu-TiO_2 could enhance the electron-hole separation effectively under visible light irradiation [68].

Er-doped tio₂

Although it is the most investigated semiconductor for heterogeneous photocatalysis, the doping with erbium has resulted in a small scientific disclosure if compared to other doping elements. Nevertheless, the structural and luminescence features of the Er-modified TiO_2 system have been extensively studied in the last years [72, 73]. It has emerged that the introduction of a small amount of Er, up to almost 2% molar, can lead an improvement in the photocatalytic ability of TiO_2, also upon visible irradiation [74, 75]; however, the mechanism governing the enhanced heterogeneous photocatalysis still requires a deeper investigation.

Different synthetic routes have been employed for the preparation of this designed material such as sol-gel [37, 76–79], hydrothermal [80–82], electrospinning [83, 84] and electrodeposition methods [85, 86], giving rise to various morphology, as reported in *Table 3*. *Zheng* et al. and *Yang* et al [83, 84]. prepared Er-doped TiO_2 nanosponges via electrospinning approach evidencing how the fibrous morphology greatly improved the photocatalytic ability in the degradation of phenol (pH) and methylene blue (MB) under visible and UV irradiation, respectively. On the other hand, a greatly improved photodegradation yield was reached by *Mazierski* et al [86]. for the photocatalytic abatement of phenol: via a electrochemical anodization techniques the authors produced oriented nanotubes that were able to almost totally mineralize the pollutant when irradiating $>$ 420 nm. Similar outcomes have been obtained by *Li et al* [85]., where the Er-TiO_2 nanotubes showed a higher photocatalytic ability respect to the bare oxide in the annihilation of methylene blue upon UV irradiation; however, high Er contempt brought to a collapse of the nano-engineered morphology.

As noticeable in *Table 3*, all the authors agree with the identification of anatase as unique phase of the crystal structure of Er-doped TiO_2 materials. The only exceptions are represented by *Zheng* et al. *and Yang* et al [83, 84]. were, in addition to anatase, also the rutile phase was detected. In the latter case, the appearance of rutile was delayed up to almost 800 °C, highlighting how the presence of erbium ions inhibited the anatase-to-rutile phase transition. They proposed that the phase transition suppression may derive from the stabilization of the anatase phase by the surrounding rare earth element through the establishment of Ti-O-Er bonds. The interaction between successive Ti atoms experiencing slightly different tetrahedral environment due to the presence of the Er would prevent the phase transformation into rutile. In any case, none of them recorded a Er_2O_3 phase via XRD analysis. Still doubts exist concerning the exact site for Er inside the anatase structure: most of the papers are in accordance with the fact that, due to the difference in the ionic radii (0.89 Å and 0.68 Å for Er^{3+} and Ti^{4+}, respectively), Er^{3+} cannot substitute a Ti^{4+} in a regular reticular site; rather it would occupy interstitial positions, or it would place at the grain boundaries. In this regard, *Reszczyńska* et al [78]. performed Rietveld analysis on the acquired XRD patterns getting no variation of the lattice parameters; conversely, *Obregon* et al [82]. obtained an increase of both *a* and *b* lattice parameters and a simultaneous decrease of *c*, so nourishing the hypothesis that Er^{3+} cations could replace Ti^{4+} or locate in interstitial cages. Accordingly, the state of the art dealing with Er-doped TiO_2 system does not clarify the structural role of erbium when it is present in the synthesis of titanium dioxide. However, XRD patterns for the Er-doped TiO_2 show a decrease in intensity of the diffractogram reflections with the increase of the Er contempt, indicating a smaller crystallite size connected to higher exposed surface area.

Actually, for the sake of completeness, it is worth citing the pioneering work of *Mignotte* et al [87]., where the solid solution $Er_yTi_xO_z$ with pyrochlore structure was assumed due to the pairing effect between the ion dopants; they attested that, due to the high amorphization of the recorded mixed phase, it cannot be identified via XRD, so justifying the absence of information on the structural role of Er in the TiO_2 matrix.

In general, UV–vis spectroscopic analysis does not evidence a marked red shift of the absorption edge for Er-doped TiO_2 compared to the pristine materials. Moreover, frequently the band gap corresponding to the different percentage of dopant amounts are not reported, as noticeable in *Table 3*. However, differently from bare TiO_2, Er-modified TiO_2 is characterized by various absorption bands in the range of visible

Table 2
Eu concentration, structure, morphology and reaction condition used for the degradation of various pollutants for different Eu-doped TiO_2 studies.

Synthetic route	Eu contempt, %	Structure and morphology	Irradiation source (Power, W)	Tested pollutant	Pollutant, concentration, mg/L	Photocatalyst, concentration, mg/L	Solution volume, mL	Best Degradation efficiency	Ref.
Precipitation using liquid phase plasma (LPP)	0.24, 0.53	Eu_2O_3 precipitated on TiO2 surface	UV LED (λ = 375 nm) and blue LED (λ = 465 nm)	Acetylsalicylic Acid (ASA)	50	500	600 mL	0.53 at%: $k = 10.65 \times 10^{-3}$ min^{-1} (UV light), $k = 1.475 \times 10^{-3}$ min^{-1} (blue light)	[63]
One step chemical green route	0.5–5	Anatase Spherical nanoparticles	UV (λ = 365 nm, 39 W) Vis-light (λ= 400–800 nm, 60 W)	MB	3.2	1000	100 mL	UV light, 0.5Eu-TiOle: 70% after 360 min. Vis light, 0.5Eu-TiOle: 90% in 240 min.	[55]
Hydrothermal	0.01–0.03	Anatase Eu doped TiO_2/Graphene Oxide Nanocomposites	UV	MB	–	500	100 mL	The 0.015% Eu^{3+}- doped TiO_2/GO photocatalyst showed the highest photocatalytic activity	[54]
Sol-gel method	1–3	Anatase Smaller nanoparticles	UV (200 W)	MB	6.4	–	–	Lower than undoped	[69]
Extraction-pyrolytic Method (EPM)	0.5–50	Anatase/rutile in different proportion according to Eu content and pyrolysis temperature Two phases of Eu_2O_3 $Eu_2Ti_2O_7$(pyrolysis T = 850 °C) Irregular rock-like agglomerates	UV–Vis light (300 W)	MB	3.6	1000	50 mL	0.5 mol% Eu, T_{pyr}= 600 °C: 96% after 60 min.	[65]
Plasma electrolytic oxidation (PEO)	–	Anatase/rutile	Vis-light (300 W)	MB	15	–	100 mL	Eu/TiO2 (410 V): 62.2% after 200 min.	[70]
Films deposition with spray pyrolysis technique	4–10	Anatase Films with tetragonal crystal structure	UV	MB	–	–	–	10 wt%: 51.5% after 180 min.	[60]
Green-chili-based biogenic method	0.5–2	Anatase polymorph Core-shell hybrid structure	UV light (λ = 300–420 nm, 24 W) vis-IR (λ = 380–950 nm, 150 W)	MB, 2-chlorophenol (2-CP)	MB: 3.2 2-CP: 5	1000	–	1.5 mol% Eu^{3+} (annealed at 600 °C): 91.5% for MB and 76.8% for 2-CP after 300 min.	[64]
Sol-gel method	0.3–1.5	Anatase Spherical particles	UV (λ = 254 nm, 15 W) Vis-light (500 W)	MB Ph	MB: 20 Phenol: 80	2000	–	0.6%Y-0.9%Eu-TiO_2: 86%, after 120 min. for MB, 53% after 120 min. for phenol	[59]
Precipitation	0.001, 0.005	Anatase Spherical particles Polycrystalline	UV (λ = 335–380 nm)	pH	47	1666	300 mL	Precipitated and sulfated TiO_2 doped with Eu (TiO_2–Eu–S): 100% after 240 min.	[52]
Microwave assisted sol-gel method	0.01–0.05	Anatase Nanoparticles	UV (λ = 365 nm) Natural sunlight	MO	–	50–200	100 mL	0.025 mol% Eu–TiO_2: 98% after 120 min.	[56]
Sol-gel mediated rapid-condensation technique	1–5	Mixture of anatase, brookite, and rutile phases (sintering temperature <600 °C) / pure anatase phase (<500 °C) Spherical particles	UV (λ = 365 nm)	MO	10	250	–	5%: 80% after 60 min.	[62]
Microwave hydrothermal method	0.02–0.12	Rutile		MO		–	–	0.08% (600 °C): 96.7%	[71]
Aqueous sol-gel process	0.10, 0.50	Anatase	UV–Vis (330 nm < l < 800 nm)	4-nitrophenol (4-NP)	14	1000	–	Lower than undoped	[58]
Microwave-hydrothermal method	0.3–1	Anatase (Eu-N) co-doped TiO_2 uniformly supported on the sepiolite Surface	Vis-light (300 W)	Orange G (OG) Real textile dye waters	OG: 10 Wastewater COD: 1654.4 after flocculation→ undiluted, diluted 1:5 and 1:10	800	150 mL	0.6% Eu: 98% after 9 h for OG 91.2% after 3 h for wastewater diluted 1:10	[67]
Sol-gel	0.5–3	Anatase Spherical or globular particles	Simulated sunlight λ = 320–780 nm	RhB	5	–	25 mL	Eu-TiO_2 (500 °C calcination) 0.5mol% Eu: 93% after 100 min.	[61]
Sol-gel impregnation method	0.5	Anatase with a minor rutile and brookite Spherical particles	Visible light (UV filter λ > 420 nm, 300 W)	RhB	20	500	200 mL	100% after 90 min.	[68]

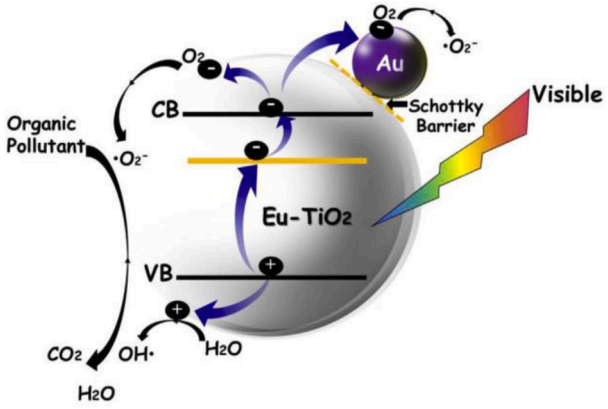

Fig. 3. Schematic reaction mechanism of visible light photocatalysis over Au/Eu-TiO_2 [68].

frequency attributable to the presence of Er^{3+} ions [75–78, 80, 81, 83, 88] Fig. 4.A) exhibits the UV–vis Kubelka-Munk absorption of different Er percentages in TiO_2 in comparison with bare TiO_2: besides to the meager absorption edge red-shift for the doped systems arising from the charge transfer transition between TiO_2 and the RE^{3+} intra-*4f* electrons or from the increasing of defect amounts, absorption peaks located at 451, 475, 524 and 655 nm also appear. These electronic transitions that fall within the visible range can be attributed to the transition from the $^4I_{15/2}$ ground state to the excited states of the erbium ions $^4F_{3/2,5/2}$, $^4F_{7/2}$, $^2H_{11/2}$ and $^4F_{9/2}$, respectively [76, 78, 84]. Obviously, the intensity of this absorption rises when increasing the Er contempt.

According to Judd–Ofelt theory of parity-forbidden electric-dipole transitions of rare earth ions, the energy states of the Er^{3+} should be effectively perturbed by the odd terms of the Hamiltonian of the weak crystal field. Despite *4f* energy electrons have been partially screened by $5s^2$ and $5p^6$ electron shells, the perturbations can still cause permitted transitions of *4f* elections between *4f* orbitals. According with the literature outcomes, this light-induced electronic transition would favor the electron-hole separation in the matrix, with a consequent increasing of the photodegradation ability [89, 90].

The behavior of the erbium species in the TiO_2 matrix developed for photocatalytic applications has been also investigated by means of PL spectroscopy. Beyond the visible emission band generated by excitation wavelength at 365 nm and deriving from the defects present in the matrix, additional emission band at specific wavelengths have been identified for Er-TiO_2 produced by an excitation pointed at 980 nm (NIR region of the electromagnetic spectrum). This outcome results from the well-known up-conversion properties of Er^{3+} ions involving a three photon absorption process and transitions from $^2H_{11/2}/^4S_{3/2}$ and $^4F_{9/2}$ excited states into $^4I_{15/2}$ ground state. Definitely, Er^{3+} ions in principle show promising photocatalytic features concerning the possibility of conversion of visible light into UV wavelengths. Finally, *Obregon* et al [82]. detected a weak UV emission in the case of NIR excitation for 2% Er-TiO_2, as reported in Fig. 4B), evidencing the feasibility to convert longer wavelengths in shorter ones, that might be absorbed by the semiconducting matrix.

Based on the structural and optical outcomes, two main working mechanisms upon light irradiation have been modelled and discussed in the examined literature. Some authors attributed the observed enhancement in the photodegradation capability of the Er-TiO_2 system to the electron scavenger action of the Er^{3+} species embedded in the anatase lattice thanks to the presence of the *4f* levels, assumed being just below the CB edge, as schematized in Fig. 5A). Er^{3+} reduces the electron-hole pairs recombination by trapping the photogenerated electron, and it is consequently reduced to Er^{2+}; this species, being unstable, gives the acquired electron to oxygen molecule that is converted in $^{\bullet}O_2^-$, capable to actively participate at the degradation process. Moreover, the photoinduced holes in the TiO_2 VB can directly oxidize a water molecule or an OH group absorbed at the surface, converting them into $^{\bullet}OH$ oxidant radicals that can attack the pollutants [77, 80, 83, 85].

The other pathways for the photoinduced charge carriers deal with

Table 3
Er concentration, structure, morphology and reaction condition used for the degradation of various pollutants for different Er-doped TiO_2 studies.

Synthetic route	Er contempt, %	Structure and morphology	Irradiation source (Power, W)	Tested pollutant	Pollutant, concentration, mg/L	Photocatalyst, concentration, mg/L	Solution volume, mL	Best Degradation efficiency	Ref.
Sol-gel	3	Anatase Macroporous films	Vis light	MB	320	–	–	100% after 1h	[76]
Electrodeposition	3	Anatase Nanotubes	UV–vis (160 W)	MB	12	–	–	95.2% after 240 min	[85]
Electrospinning	0.5–1.5	Anatase. Anatase and Rutile for temperatures greater than 773 K. Nanofibrous films	UV–vis (500 W)	MB	12.8	250	400 mL	1% Er, 75% after 180 min	[84]
Sol-gel	0.1	Anatase	UV-light (10 W)	MB	15	2500	100 mL	80% after 2h	[79]
Sol-gel	0.5–2	Anatase	Vis-light (70 W)	MO	19.6	1000	250 mL	1.5% Er, 80% after 1h	[77]
Sol-gel	–	Anatase	UV–vis (λ_{max} = 365 nm,200 W)	N-(1-naphthyl)	0.12	1000	–	50% after 1h	[88]
Hydrothermal	5	Anatase	UV–vis	pH	20	–	–	–	[80]
Electrochemical anodization	0.025	Anatase Nanotubes	Vis-light ($\lambda \geq 420$ nm)	pH	20	–	25 mL	80% after 1h	[86]
Hydrothermal	0.5–4	Anatase	UV–vis	pH	–	–	–	2% Er, 90% after 2 h	[81]
Hydrothermal	0.5–4	Anatase	UV–vis (200 W)	pH	30	1000	250 mL	2% Er, 90% after 2h	[82]
Sol-gel	0.25–1	Anatase	Vis-light (200 W)	pH	19.7	10,000	5 mL	0.5% Er, 80% after 180 min	[78]
Electrospinning	0.5–5	Anatase. Anatase and Rutile for 5% mol Er. Sponge nanofibers	LED light (λ = 517–522 nm,3 W)	RhB, Ph	RhB: 48 pH: 20	1000	50 mL	0.5% Er, 90%after 10 h for RhB. 0.5% Er, 50% after 70 h for Ph.	[83]

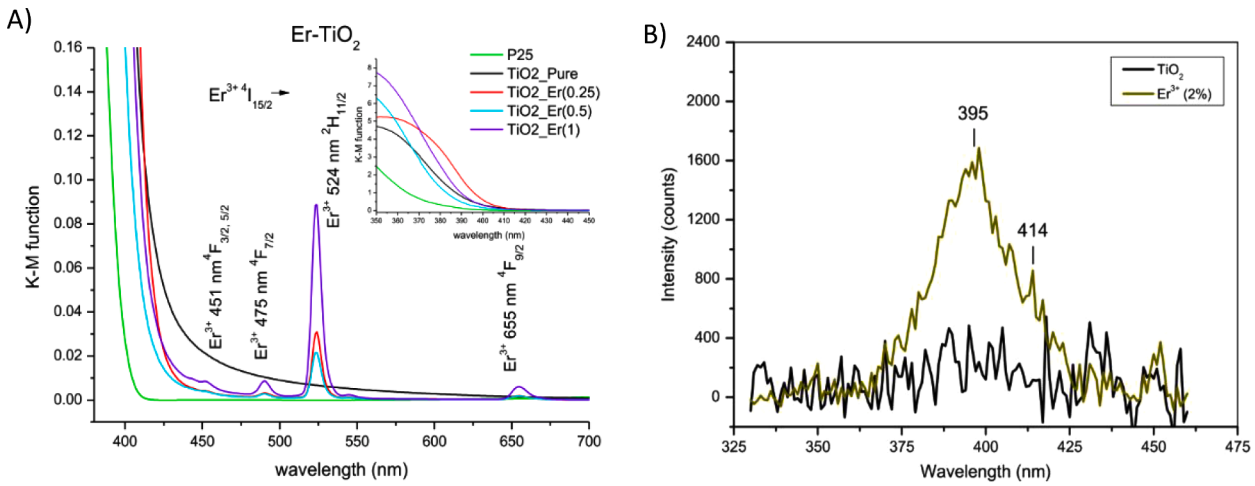

Fig. 4. A): Comparison of the UV–vis Kubelka–Munk absorption of pure TiO_2 and different%Er-TiO_2 photocatalysts [78]. B): UV Er^{3+} luminescent spectra under λ_{ex} = 980 nm excitation [82]..

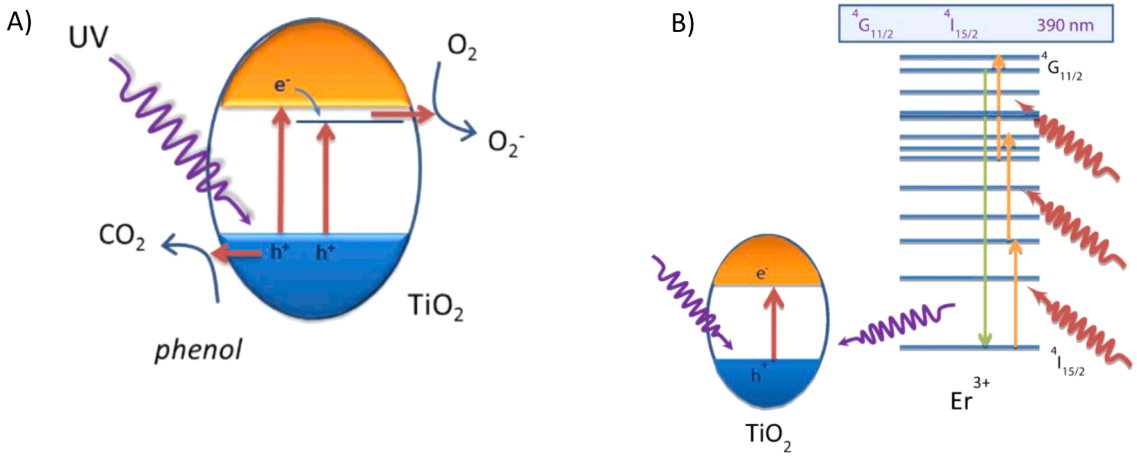

Fig. 5. Different proposed working mechanism for the%Er-TiO_2 photocatalysts: A) under UV excitation and B)NIR excitation [82]..

the already mentioned up-conversion process characterizing Er^{3+} ions, with the absorption of NIR photons and the subsequent pumping of visible and UV photons. The up-conversion process would involve a sequential three-photons absorption ($^4I_{15/2}$ →$^4I_{11/2}$, $^4I_{11/2}$→$^4F_{7/2}$ and $^4S_{3/2}$→$^2G_{7/2}$). In this way, via a multiphoton relaxation the $^2G_{7/2}$ excited state decays to $^2G_{11/2}$ and $^2H_{9/2}$ lower states. The UV-violet emission around 390 nm would then be produced by $^2G_{11/2}$ to the $^4I_{15/2}$ ground state. Finally, the improvement in the photo-efficiency might be related to the increased number of available photons in the UV spectral range that can be absorbed by TiO_2 matrix for the generation of electron-hole pairs, as depicted in Fig. 5B) [76, 82].

However, it is worth mentioning that the up-conversion mechanism impact on the improvement of the photodegradation of harmful pollutants in wastewater of Er-TiO_2 has not yet experimentally evidenced. For this region, further investigations are required in the future for clarifying this aspect. In addition, no information is available on the role of the pyrochlore phase in the enhancement of the photons' absorption in visible range and in the higher photocatalytic activity.

Conclusions

The current review offers an overview of the most recent studies concerning the introduction of three selected lanthanoids, namely cerium, europium and erbium, in the semiconductor oxide TiO_2 with the aim of increasing its photocatalytic efficiency in the removal of pollutants from wastewater and surface water.

Literature data suggest that the modification of titanium dioxide with the considered lanthanoids (Ln) is an effective strategy to increase the photocatalytic activity, especially when the optimal doping percentage is identified, since it affects, among others, its structural role. In fact, in some studies the lanthanoid has been disclosed inside the crystal lattice of the oxide, even if the difference in symmetry and ion radius size makes the formation of a biphasic solid characterized by the presence of Ln_2O_3 on the surface of the titanium dioxide more plausible.

Ln(III) doping increases the number of surface defects such as oxygen vacancies on the material surface, which act as traps for the photogenerated charge carriers resulting in a reduction of their recombination rate. In addition, the introduction of lanthanoids leads to an inhibition of the transition from the anatase to rutile phase, that is desirable as the former is known to possess a higher photocatalytic activity.

Furthermore, one of the most noteworthy improvements is the increased absorption of visible light noted for these materials that makes them particularly attractive for an eco-sustainable removal of contaminants from water.

Unfortunately, the extreme heterogenicity of operating conditions, such as the type of synthesis, the lighting system and the pollutant and catalyst concentrations, make a direct comparison between the materials of the various studies very complex. Therefore, it is not possible to define which is the most promising lanthanoid for the doping of TiO_2 and in this regard it would be very interesting to perform a comparative

study that clarifies this aspect.

Moreover, although there are now numerous studies regarding these photocatalysts in the literature, the study of photocatalytic activity is often carried out on a narrow range of organic molecules and is not exhaustively related to the role that lanthanoids could actually partake. For example, it would be interesting and useful to investigate whether the presence of the pyrochlore structure that has been observed in some studies may be a source of the photocatalytic activity of Ce/Eu /Er-doped-TiO_2 materials.

The evaluation of the photoactivity of Ln doped TiO_2 is at present largely performed on dyes and, for such, further studies exploring their feasibly toward CECs abatement are required. Besides, in order to optimize time and costs required for the experimental tests, the combination with a theoretical approach and computational calculations would be beneficial.

Declaration of interests

The authors declare that they have no known competing financial interests or personal relationships that could have appeared to influence the work reported in this paper.

Acknowledgement

This paper is part of a project that has received funding from the European Union's Horizon 2020 research and innovation program under the Marie Skłodowska-Curie grant agreement no. 765860 (AQUAlity), from the European Union's Horizon 2020 research and innovation program under the Marie Skłodowska-Curie grant agreement No 101007578″ (SusWater) and from the Italian MIUR through the PRIN Project 20179337R7, MULTI-e "Multielectron transfer for the conversion of small molecules: an enabling technology for the chemical use of renewable energy"; Compagnia di San Paolo and University of Torino are gratefully acknowledged for funding "Bando per il finanziamento ex-post di progetti di ricerca di Ateneo anno 2018″

References

[1] O. Golovko, S. Örn, M. Sörengård, K. Frieberg, W. Nassazzi, F.Y. Lai, L. Ahrens, Occurrence and removal of chemicals of emerging concern in wastewater treatment plants and their impact on receiving water systems, Sci. Total Environ. 754 (2021), 142122.

[2] K.A. Baken, R.M. Sjerps, M. Schriks, A.P. van Wezel, Toxicological risk assessment and prioritization of drinking water relevant contaminants of emerging concern, Environ. Int. 118 (2018) 293–303.

[3] T.K. Kasonga, M.A. Coetzee, I. Kamika, V.M. Ngole-Jeme, M.N.B. Momba, Endocrine-disruptive chemicals as contaminants of emerging concern in wastewater and surface water: a review, J. Environ. Manage. 277 (2021), 111485.

[4] G. Matafonova, V. Batoev, Recent advances in application of UV light-emitting diodes for degrading organic pollutants in water through advanced oxidation processes: a review, Water Res. 132 (2018) 177–189.

[5] J. Li, Y. Li, Z. Xiong, G. Yao, B. Lai, The electrochemical advanced oxidation processes coupling of oxidants for organic pollutants degradation: a mini-review, Chin. Chem. Lett. 30 (2019) 2139–2146.

[6] A. Machulek Jr, S.C. Oliveira, M.E. Osugi, V.S. Ferreira, F.H. Quina, R.F. Dantas, S. L. Oliveira, G.A. Casagrande, F.J. Anaissi, V.O. Silva, Application of different advanced oxidation processes for the degradation of organic pollutants, Organic pollutants-Monitoring, risk and treatment, InTech. (2013) 141–166.

[7] M.J. López-Muñoz, J. Aguado, A. Arencibia, R. Pascual, Mercury removal from aqueous solutions of HgCl2 by heterogeneous photocatalysis with TiO2, Appl. Catal. B 104 (2011) 220–228.

[8] C. Belver, J. Bedia, A. Gómez-Avilés, M. Peñas-Garzón, J.J. Rodriguez, Chapter 22 - Semiconductor Photocatalysis for Water Purification, in: S. Thomas, D. Pasquini, S.-Y. Leu, D.A. Gopakumar (Eds.), Nanoscale Materials in Water Purification, Elsevier, 2019, pp. 581–651.

[9] S. Cassaignon, C. Colbeau-Justin, O. Durupthy, Titanium Dioxide in Photocatalysis, Nanomaterials: A Danger or a Promise? (2013) 153–188.

[10] N.U. Saqib, R. Adnan, I. Shah, A mini-review on rare earth metal-doped TiO2 for photocatalytic remediation of wastewater, Environ. Sci. Pollut. Res. Int. 23 (2016) 15941–15951.

[11] M.A. Barakat, R. Kumar, Photocatalytic activity enhancement of Titanium Dioxide Nanoparticles, Photocatalytic Activity Enhancement of Titanium Dioxide Nanoparticles (2016) 1–29.

[12] G. Qin, Z. Sun, Q. Wu, L. Lin, M. Liang, S. Xue, Dye-sensitized TiO2 film with bifunctionalized zones for photocatalytic degradation of 4-cholophenol, J. Hazard. Mater. 192 (2011) 599–604.

[13] P. Chowdhury, J. Moreira, H. Gomaa, A.K. Ray, Visible-solar-light-driven photocatalytic degradation of phenol with dye-sensitized TiO2: parametric and Kinetic study, Ind. Eng. Chem. Res. 51 (2012) 4523–4532.

[14] V. Subramanian, E. Wolf, P.V. Kamat, Semiconductor−metal composite nanostructures. to what extent do metal nanoparticles improve the photocatalytic activity of TiO2 films? J. Phys. Chem. B 105 (2001) 11439–11446.

[15] S. Sakthivel, M.V. Shankar, M. Palanichamy, B. Arabindoo, D.W. Bahnemann, V. Murugesan, Enhancement of photocatalytic activity by metal deposition: characterisation and photonic efficiency of Pt, Au and Pd deposited on TiO2 catalyst, Water Res. 38 (2004) 3001–3008.

[16] V. Bhatia, A. Dhir, Transition metal doped TiO2 mediated photocatalytic degradation of anti-inflammatory drug under solar irradiations, J. Environ. Chem. Eng. 4 (2016) 1267–1273.

[17] P. Karuppasamy, N. Ramzan Nilofar Nisha, A. Pugazhendhi, S. Kandasamy, S. Pitchaimuthu, An investigation of transition metal doped TiO2 photocatalysts for the enhanced photocatalytic decoloration of methylene blue dye under visible light irradiation, J. Environ. Chem. Eng. 9 (2021), 105254.

[18] A.D. Paola, S. Ikeda, G. Marcì, B. Ohtani, L. Palmisano, Transition metal doped TiO_2: physical properties and photocatalytic behaviour, Int. J. Photoenergy 3 (2001), 370924.

[19] T. Tang, Z. Yin, J. Chen, S. Zhang, W. Sheng, W. Wei, Y. Xiao, Q. Shi, S. Cao, Novel p-n heterojunction Bi2O3/Ti3+-TiO2 photocatalyst enables the complete removal of tetracyclines under visible light, Chem. Eng. J. 417 (2021), 128058.

[20] Y. Xue, Z. Wu, X. He, X. Yang, X. Chen, Z. Gao, Constructing a Z-scheme Heterojunction of Egg-Like Core@shell CdS@TiO2 Photocatalyst via a Facile Reflux Method for Enhanced Photocatalytic Performance, Nanomaterials 9 (2019).

[21] Y. Liu, S. Ding, J. Xu, H. Zhang, S. Yang, X. Duan, H. Sun, S. Wang, Preparation of a p-n heterojunction BiFeO3@TiO2 photocatalyst with a core–shell structure for visible-light photocatalytic degradation, Chin. J. Catal. 38 (2017) 1052–1062.

[22] D. Wu, M. Long, W. Cai, C. Chen, Y. Wu, Low temperature hydrothermal synthesis of N-doped TiO2 photocatalyst with high visible-light activity, J. Alloys Compd. 502 (2010) 289–294.

[23] H. Li, Y. Hao, H. Lu, L. Liang, Y. Wang, J. Qiu, X. Shi, Y. Wang, J. Yao, A systematic study on visible-light N-doped TiO2 photocatalyst obtained from ethylenediamine by sol–gel method, Appl. Surf. Sci. 344 (2015) 112–118.

[24] T. Umebayashi, T. Yamaki, H. Itoh, K. Asai, Band gap narrowing of titanium dioxide by sulfur doping, Appl. Phys. Lett. 81 (2002) 454–456.

[25] G.B. Vieira, G. Scaratti, F.S. Rodembusch, S.M. De Amorim, M. Peterson, G. Li Puma, R. Muniz-Moreira, Tuning the Photoactivity of TiO_2 Nanoarchitectures doped with Cerium or Neodymium and application to color removal from wastewaters, Environ. Technol. 42 (2021) 1038–1052.

[26] A. Makdee, P. Unwiset, K.C. Chanapattharapol, P. Kidkhunthod, Effects of Ce Addition on the Properties and Photocatalytic Activity of TiO_2, Investigated by X-ray Absorption Spectroscopy, Mater. Chem. Phys. 213 (2018) 431–443.

[27] L. Gong, Z. Zhou, A.S. Wang, B. Wang, Preparation and characterization of cerium-doped titanium dioxide/ultrahigh-molecular-weight polyethylene porous composites with excellent photocatalytic activity, J. Appl. Polym. Sci. 129 (2013) 1212–1217.

[28] T. Tong, J. Zhang, B. Tian, F. Chen, D. He, M. Anpo, Preparation of Ce–TiO_2 Catalysts by Controlled Hydrolysis of Titanium Alkoxide based on Esterification reaction and study on its photocatalytic activity, J. Colloid Interface Sci. 315 (2007) 382–388.

[29] P. Sun, L. Liu, S. Cui, J. Liu, Synthesis, Characterization of Ce-doped TiO_2 Nanotubes with high visible light photocatalytic activity, Catal. Lett. 144 (2014) 2107–2113.

[30] B. Wang, F. Condi de Godoi, S. Zheng, I.R. Gentle, C. Li, Enhanced photocatalytic properties of reusable TiO_2-loaded natural porous minerals in dye wastewater purification, Powder Technol. 302 (2016) 426–433.

[31] K. Kasinathan, J. Kennedy, M. Elayaperumal, M. Henini, M. Malik, Photodegradation of Organic Pollutants RhB Dye using UV simulated sunlight on ceria based TiO_2 nanomaterials for antibacterial applications, Sci. Rep. 6 (2016) 1–12.

[32] B. Choudhury, B.B.A. Choudhury, Extending photocatalytic activity of TiO_2 nanomaterials: a danger or a promise? abbreviation, Photochem. Photobiol. 88 (2012) 257–264.

[33] T. Ma, J. Cao, G. Shao, X. Zhang, Z. Yuan, Hierarchically structured squama-like Cerium-Doped Titania: synthesis, Photoactivity, and Catalytic CO Oxidation, J. Phys. Chem. C 113 (2009) 16658–16667.

[34] Z. Duan, Q. Li, X. Zhao, Z. Peng, S. Zhang, Photocatalytic degradation of methyl orange on Ce-TiO_2 under visible light irradiation, Adv. Mater. Res. 529 (2012) 528–531.

[35] I.T. Liu, M.-.H. Hon, L.G. Teoh, The preparation, characterization and photocatalytic activity of radical-shaped CeO_2/ZnO microstructures, Ceram. Int. 40 (2014) 4019–4024.

[36] S. Yao, Y. Yang, S. Song, Z. Shi, Preparation, characterization and photocatalytic activity of cerium-doped titanium dioxide supported on activated carbon fiber composite, Indian J. Chem. 53A (2014) 665–671.

[37] J. Xu, Y. Ao, D. Fu, C. Yuan, Study on photocatalytic performance and degradation kinetics of x-3b with lanthanide-modified titanium dioxide under solar and UV illumination, J. Hazard. Mater. 164 (2009) 762–768.

[38] J. Santiago-Morales, M.J. Gomez, S. Herrera-Lopez, A.R. Fernandez-Alba, E. García-Calvo, R. Rosal, Energy efficiency for the removal of non-polar pollutants

during ultraviolet irradiation, visible light photocatalysis and ozonation of a wastewater effluen, Water Res. 47 (2013) 5546–5556.
[39] F.B. Li, X.Z. Li, M.F. Hou, K.W. Cheah, W.C.H. Choy, Enhanced photocatalytic activity of Ce^{3+}–TiO_2 for 2-mercaptobenzothiazole degradation in aqueous suspension for odour control, Appl. Catal., A 285 (2005) 181–189.
[40] N. Shaari, S.H. Tan, A.R. Mohamed, Synthesis and characterization of CNT/Ce-TiO_2 nanocomposite for Phenol degradation, J. Rare Earths 30 (2012) 651–658.
[41] P. He, Z. Zhao, Y. Tan, E. Hengchao, M. Zuo, J. Wang, J. Yang, S. Cui, X. Yang, Photocatalytic degradation of deoxynivalenol using cerium doped titanium dioxide under ultraviolet light irradiation, Toxins (Basel) 13 (2021) 481–494.
[42] W. Xue, G. Zhang, X. Xu, X. Yang, C. Liu, Y. Xu, Preparation of Titania nanotubes doped with cerium and their photocatalytic activity for glyphosate, Chem. Eng. J. 167 (2011) 397–402.
[43] L. Behera, B. Barik, S. Mohapatra, Improved Photodegradation and antimicrobial activity of hydrothermally synthesized 0.2Ce-TiO_2/RGO under visible light, Colloids Surf., A 620 (2021) 1265531–12655312.
[44] F. Galindo, R. Gómez, M. Aguilar, Photodegradation of the Herbicide 2,4-Dichlorophenoxyacetic Acid on Nanocrystalline TiO_2–CeO_2 Sol–Gel Catalysts, J. Mol. Catal. A: Chem. 281 (2008) 119–125.
[45] T. López, F. Rojas, R. Alexander-Katz, F. Galindo, A. Balankin, A. Buljan, Porosity, structural and fractal study of Sol–Gel TiO_2–CeO_2 mixed oxides, J. Solid State Chem. 177 (2004) 1873–1885.
[46] J. Fang, X. Bi, D. Si, Z. Jiang, W. Huang, Spectroscopic studies of interfacial structures of CeO2–TiO2 mixed oxides, Appl. Surf. Sci. 253 (2007) 8952–8961.
[47] Z. Liu, B. Guo, L. Hong, H. Jiang, Preparation and Characterization of Cerium Oxide doped TiO_2 Nanoparticles, J. Phys. Chem. Solids 66 (2005) 161–167.
[48] J. Liu, H. Li, Q. Li, X. Wang, M. Zhang, J. Yang, Preparation of cerium modified titanium dioxide nanoparticles and investigation of their visible light photocatalytic performance, Int. J. Photoenergy (2014) 1–9.
[49] G.B. Vieira, G. Scaratti, F.S. Rodembusch, S.M. De Amorim, M. Peterson, G. L. Puma, R. Moreira, Tuning the photoactivity of TiO2 nanoarchitectures doped with cerium or neodymium and application to colour removal from wastewaters, Environ. Technol. 42 (2021) 1038–1052.
[50] C. Gionco, M.C. Paganini, S. Agnoli, A.E. Reederb, E. Giamello, Structural and spectroscopic characterization of CeO_2-TiO_2 mixed oxides, J. Mater. Chem. A (2013) 10918–10926.
[51] M. Martos, B. Julián-López, J.V. Folgado, E. Cordoncillo, P. Escribano, Sol–Gel synthesis of tunable cerium Titanate materials, Eur. J. Inorg. Chem. 2008 (2008) 3163–3171.
[52] R. Michal, E. Dworniczek, M. Čaplovičová, M. Gregor, L.u. Čaplovič, A. Seniuk, P. Kuš, G. Plesch, Photocatalytic and photodisinfectant activity of sulfated and Eu doped anatase against clinically important microorganisms, Ceram. Int. 40 (2014) 5745–5756.
[53] C. Leostean, M. Stefan, O. Pana, A.I. Cadis, R.C. Suciu, T.D. Silipas, E. Gautron, Properties of Eu doped TiO2 nanoparticles prepared by using organic additives, J. Alloys Compd. 575 (2013) 29–39.
[54] M.S. Gohr, H.S. Hafez, M.M. Saif, H.M.A. Soliman, M.S.A. Abdel-Mottaleb, Facile hydrothermal synthesis of Sm and Eu doped TiO2/graphene oxide nanocomposites for photocatalytic applications, Egypt. J. Chem. 63 (2020) 1359–1382.
[55] D. Caschera, F. Federici, T. de Caro, B. Cortese, P. Calandra, A. Mezzi, R. Lo Nigro, R.G. Toro, Fabrication of Eu-TiO2 NCs functionalized cotton textile as a multifunctional photocatalyst for dye pollutants degradation, Appl. Surf. Sci. 427 (2018) 81–91.
[56] G.V. Khade, N.L. Gavade, M.B. Suwarnkar, M.J. Dhanavade, K.D. Sonawane, K. M. Garadkar, Enhanced photocatalytic activity of europium doped TiO2 under sunlight for the degradation of methyl orange, J. Mater. Sci. Mater. Electron. 28 (2017) 11002–11011.
[57] N.R. Khalid, M. Liaqat, M.B. Tahir, G. Nabi, T. Iqbal, N.A. Niaz, The role of graphene and europium on TiO2 performance for photocatalytic hydrogen evolution, Ceram. Int. 44 (2018) 546–549.
[58] C.M. Malengreaux, S.L. Pirard, G. Léonard, J.G. Mahy, M. Herlitschke, B. Klobes, R. Hermann, B. Heinrichs, J.R. Bartlett, Study of the photocatalytic activity of Fe3+, Cr3+, La3+ and Eu3+ single-doped and co-doped TiO2 catalysts produced by aqueous sol-gel processing, J. Alloys Compd. 691 (2017) 726–738.
[59] R. Wang, F. Wang, S. An, J. Song, Y. Zhang, Y/Eu co-doped TiO2: synthesis and photocatalytic activities under UV-light, J. Rare Earths 33 (2015) 154–159.
[60] S.M. Al-Shomar, Synthesis and characterization of Eu3+ doped TiO2 thin films deposited by spray pyrolysis technique for photocatalytic application, Mater. Res. Express 8 (2021).
[61] D.S. Zhen, M. Guo, X.F. Li, H.L. Mao, C.A. Li, J.L. Li, Y. Liu, Eu-TiO(2) nanocomposite with high photoelectrochemical activity for enhanced photocatalysis of rhodaminee B, J. Nanosci. Nanotechnol. 19 (2019) 7758–7763.
[62] N. Paul, D. Mohanta, Effective optoelectronic and photocatalytic response of Eu3+-doped TiO2 nanoscale systems synthesized via a rapid condensation technique, J. Mater. Res. 28 (2013) 1471–1480.
[63] S.-.C. Jung, H.-.J. Bang, H. Lee, H.-.H. Ha, Y.H. Yu, S.-.J. Kim, Y.-.K. Park, Assessing the photocatalytic activity of europium doped TiO2 using liquid phase plasma process on acetylsalicylic acid, Catal. Today (2020).
[64] P.V. Rajeswari, S. Ram, D. Pradhan, Core-shell synergy and Eu3+ doping in boosting charge transfer in Eu3+ doped TiO2-carbon core-shell nanohybrids: sustainable synthesis and visible light-driven photocatalysis, Appl. Surf. Sci. 492 (2019) 473–486.
[65] V. Serga, R. Burve, A. Krumina, V. Pankratova, A.I. Popov, V. Pankratov, Study of phase composition, photocatalytic activity, and photoluminescence of TiO2 with Eu additive produced by the extraction-pyrolytic method, J. Mater. Res. Technol. 13 (2021) 2350–2360.
[66] Z. Jiang, Y. Lin, T. Mei, X. Hu, W. Chen, R. Ji, E. Liu, R. Zhang, L. Zhang, Q. Zhang, B. Zhou, D. Zhang, J. Fan, H. Zhu, X. Zhang, S. Wan, S. Zhu, Y. Shang, First-principles study of the electronic and optical properties of the (Eu,N)-codoped anatase TiO2 photocatalyst, Comput. Mater. Sci. 68 (2013) 234–237.
[67] F. Zhou, H. Wang, S. Zhou, Y. Liu, C. Yan, Fabrication of europium-nitrogen co-doped TiO2/Sepiolite nanocomposites and its improved photocatalytic activity in real wastewater treatment, Appl. Clay Sci. 197 (2020), 105791.
[68] X. Lin, H. Chen, Z. Hu, Y. Hou, W. Dai, Enhanced visible light photocatalysis of TiO2 by Co-modification with Eu and Au nanoparticles, Solid State Sci. 83 (2018) 181–187.
[69] J. Vargas Hernández, S. Coste, A. García Murillo, F. Carrillo Romo, A. Kassiba, Effects of metal doping (Cu, Ag, Eu) on the electronic and optical behavior of nanostructured TiO2, J. Alloys Compd. 710 (2017) 355–363.
[70] Y. Shi, J. Li, Z. Yu, X. Yuan, Investigation of enhanced photocatalytic performance of europium doped TiO2 film, Mater. Technol. 36 (2020) 552–563.
[71] Y. Yi, C. Chen, X. Bi, Preparation of Eu-doped TiO2 Photocatalyst by Microwave Hydrothermal Method and its Photocatalytic Activity, in: 2019 2nd Scientific Workshop on Chemical and Agricultural Sciences (SWCAS 2019), 2019.
[72] J. Zhang, X. Wang, W.-.T. Zheng, X.-.G. Kong, Y.-.J. Sun, X. Wang, Structure and luminescence properties of TiO_2:er^{3+} nanocrystals annealed at different temperatures, Mat. Lett. 61 (2007) 1658–1661.
[73] X. Mao, B. Yan, J. Wang, J. Shen, Up-Conversion Fluorescence characteristics and mechanism of Er^{3+}-doped TiO_2 thin films, Vacuum 102 (2014) 38–42.
[74] A.S. Weber, A.M. Grady, R.T. Koodali, Lanthanide modified semiconductor photocatalysts, Catal. Sci. Technol. 2 (2012) 683.
[75] P. Mazierski, A. Mikolajczyk, B. Bajorowicz, A. Malankowska, A. Zaleska-Medynska, J. Nadolna, The role of lanthanides in TiO_2-based photocatalysis: a review, Appl. Catal., B 233 (2018) 301–317.
[76] J. Castañeda-Contreras, V.F. Marañón-Ruiz, R. Chiu-Zárate, H. Pérez-Ladrón de Guevara, R. Rodriguez, C. Michel-Uribe, Photocatalytic activity of Erbium-doped TiO_2 nanoparticles immobilized in macro-porous silica films, Mater. Res. Bull. 47 (2012) 290–295.
[77] C.H. Liang, M.F. Hou, S.G. Zhou, F.B. Li, C.S. Liu, T.X. Liu, Y.X. Gao, X.G. Wang, J. L. Lu, The effect of erbium on the adsorption and photodegradation of orange I in Aqueous Er^{3+}-TiO_2 suspension, J. Hazard. Mater. 138 (2006) 471–478.
[78] J. Reszczyńska, T. Grzyb, J.W. Sobczak, W. Lisowski, M. Gazda, B. Ohtani, A. Zaleska, Visible light activity of rare earth metal doped (Er3+, Yb3+ or Er3+/Yb3+) Titania Photocatalysts, Appl. Catal., B 163 (2015) 40–49.
[79] X. Xu, B. Fang, F. Zhang, Y. Tian, J. Wu, Influence of rare earth co-dopant on the photocatalytic property of TiO2 nano-particles, J. Wuhan Univ. Technol.-Mater. Sci. Ed. 25 (2010) 370–374.
[80] X. Fang, X. Chen, Z. Zhu, Optical and Photocatalytic Properties of Er^{3+} and/or Yb^{3+} doped TiO_2 Photocatalysts, J. Mater. Sci.: Mater. Electron. 28 (2016) 474–479.
[81] S. Obregon, G. Colon, Evidence of upconversion luminescence contribution to the improved photoactivity of Erbium doped TiO_2 Systems, Chem. Commun. 48 (2012) 7865–7867.
[82] S. Obregón, A. Kubacka, M. Fernández-García, G. Colón, High-Performance Er^{3+}–TiO_2 System: dual Up-conversion and electronic role of the lanthanide, J. Catal. 299 (2013) 298–306.
[83] Y. Zheng, W. Wang, Electrospun nanofibers of Er3+-doped TiO2 with photocatalytic activity beyond the absorption edge, J. Solid State Chem. 210 (2014) 206–212.
[84] Y. Yang, C. Zhang, Y. Xu, H. Wang, X. Li, C. Wang, Electrospun Er, TiO2 nanofibrous films as efficient photocatalysts under solar simulated light, Mater. Lett. 64 (2010) 147–150.
[85] Y. Li, Y. Wang, J. Kong, J. Wang, Synthesis and photocatalytic activity of TiO2 nanotubes Co-doped by erbium ions, Appl. Surf. Sci. 328 (2015) 115–119.
[86] P. Mazierski, W. Lisowski, T. Grzyb, M.J. Winiarski, T. Klimczuk, A. Mikołajczyk, J. Flisikowski, A. Hirsch, A. Kołakowska, T. Puzyn, A. Zaleska-Medynska, J. Nadolna, Enhanced photocatalytic properties of lanthanide-TiO_2 nanotubes: an experimental and theoretical study, Appl. Catal., B 205 (2017) 376–385.
[87] C. Mignotte, EXAFS studies on Erbium-doped TiO_2 and ZrO_2 Sol-gel thin films, J. Non-Cryst. Solids 291 (2001) 56–77.
[88] A.-.W. Xu, Y. Gao, H.-.Q. Liu, The preparation, characterization, and their photocatalytic activities of rare-earth-doped TiO2 Nanoparticles, J. Catal. 207 (2002) 151–157.
[89] R. Salhi, J.-.L. Deschanvres, Efficient green and red up-conversion emissions in Er/Yb co-doped TiO_2 Nanopowders prepared by hydrothermal-assisted Sol–gel process, J. Lumin. 176 (2016) 250–259.
[90] J. Méndez-Ramos, P. Acosta-Mora, J.C. Ruiz-Morales, T. Hernández, M.E. Borges, P. Esparza, Turning into the Blue: materials for Enhancing TiO_2 Photocatalysis by Up-Conversion Photonics, RSC Adv. 3 (2013) 23028.